Journal of Alloys and Compounds 732 (2018) 280–285

Contents lists available at ScienceDirect

Journal of Alloys and Compounds

journal homepage: http://www.elsevier.com/locate/jalcom

Pressure-induced structural transitions and electronic topological transition of Cu_2Se

Yuhang Zhang [a, b], Xuecheng Shao [a], Yanbin Zheng [a, c], Limin Yan [a], Pinwen Zhu [a, *], Yan Li [a, **], Huailiang Xu [b, ***]

[a] State Key Laboratory of Superhard Materials, College of Physics, Jilin University, Changchun, 130012, China
[b] State Key Laboratory on Integrated Optoelectronics, College of Electronic Science and Engineering, Jilin University, Changchun, 130012, China
[c] Changchun University of Chinese Medicine, Changchun, 130012, China

ARTICLE INFO

Article history:
Received 14 June 2017
Received in revised form
14 October 2017
Accepted 23 October 2017
Available online 2 November 2017

Keywords:
Cu_2Se
High-pressure
Structural transition
Electronic topological transition

ABSTRACT

We performed high-pressure *in situ* angle dispersive X-ray diffraction (ADXRD) experiments combined with CALYPSO methodology and band structure calculations on Cu_2Se up to 42.1 GPa at room temperature, and four phases were identified. The initial low-pressure phase is assigned to the previously proposed monoclinic structure (space group $C2/c$). Phase II (space group $C2/m$) and phase III (space group $C2/m$) emerged at 3.3 GPa. Moreover, a bulk metallic phase IV (space group $Pca2_1$) emerged at 7.4 GPa. We find that, unexpectedly, semimetallic phase III probably experiences a pressure-induced electronic topological transition (ETT) to another semimetallic state at about 20.0–25.0 GPa. Our results show that pressure plays a dramatic role in tuning Cu_2Se's crystal structures and electronic states.

1. Introduction

Copper selenide as an important member of the transition metal chalcogenides (TMCs) has received heightened attention for various interesting properties. Recently, thanks to the extremely low thermal conductivity, thermoelectric figure of merit *ZT* value of 1.5 was achieved in the superionic $Cu_{2-x}Se$ at 1000 K [1,2]. Moreover, by utilizing critical electron and phonon scattering, a dramatic *ZT* value of 2.3 was shown in iodine-doped Cu_2Se at 400 K [3]. Additionally, the recent transport property measurements exhibited the extraordinary weak anti-localization type of magnetoresistance in Cu_2Se at liquid nitrogen temperatures, which confirmed the existence of a possible CDW state at low temperature [4]. It is known that Cu_2Se is an indirect band-gap semiconductor (Eg~1.25–1.5 eV) under ambient conditions [5]. Moreover, at about 400 K, it experiences a reversible second-order structural transition to a superionic state with simple antifluorite structure (space group Fm-$3m$) [6–13]. However, the room-temperature crystal structure of Cu_2Se remains controversial. Therefore, many structural models were theoretically proposed, including several monoclinic structures with space group $P2_1/c$ and $C2/c$, respectively [3,4,14].

Pressure can provide the cleanest route to tune the crystalline structures and physical properties of the TMCs. For examples, pressure-induced ETT, a modification of the topology of the Fermi surface, can result in pronounced increase of thermoelectric properties in these compounds [15–24]. Besides, pressure significantly raises the superconducting transition temperature T_c in almost established CDW compounds [25–36]. Furthermore, several members of chalcogenides, such as α-Bi_2Se_3, α-Bi_2Te_3, α-Sb_2Te_3, β-Ag_2Te and β-Ag_2Se, have been theoretically proposed and experimentally exhibited as three-dimensional topological insulators (TIs) [37–45]. In addition, Murray et al. reported that Cu_2Se undergoes a structural transition at about 4.0 GPa, while the structure of the high-pressure phase is still unknown [46]. Therefore, it is important to explore the crystalline structures and intriguing physical properties of Cu_2Se upon pressure.

Here, we report the pressure-induced phase transition sequence for Cu_2Se by *in-situ* high-pressure ADXRD measurements, using a diamond anvil cell (DAC), in conjunction with first-principles calculations.

* Corresponding author.
** Corresponding author.
*** Corresponding author.
E-mail addresses: zhupw@jlu.edu.cn (P. Zhu), liyan2012@jlu.edu.cn (Y. Li), huailiang_xu@jlu.edu.cn (H. Xu).

https://doi.org/10.1016/j.jallcom.2017.10.201
0925-8388/

2. Experimental details

In our experiments, polycrystalline Cu_2Se samples were prepared following the recipes described elsewhere [47]. *In situ* high-pressure ADXRD data was collected at the beamline BL15U1 of the Shanghai Synchrotron Radiation Facility (SSRF) with a wavelength of 0.6199 Å. The ADXRD experiments were conducted up to 42 GPa using methanol-ethanol-water (16:3:1) mixture, so considerable non-hydrostatic conditions are expected above 20–25 GPa. The integration to conventional 2θ-intensity data was carried out with the FIT2D software [48]. Rietveld refinements were performed using the GSAS-EXPGUI package [49,50].

To determine high-pressure structures, we used a global minimization of free energy surfaces merging *ab initio* total-energy calculations via CALYPSO methodology [51]. For the first-principles calculations, the density functional theory with the Perdew-Burke-Ernzerhof exchange-correlation as implemented in the Vienna Ab initio Simulation Package (VASP) code [52] and the generalized gradient approximation (GGA) [53] is implemented on a projector augmented wave (PAW) basis [54,55]. The PAW method based upon the frozen core approximation with $3d^{10}4s^1$ and $4s^24p^4$ electrons as valence for Cu and Se, respectively, was adopted. In order to obtain very well converged energies, a $4 \times 4 \times 4$ grid of special k-points was employed for the integration over the Brillouin zone (BZ) with a kinetic energy cutoff of 300 eV, ensuring convergence of the total energy within 10^{-3} meV/atom. In order to compare with experimental results, the structures were fully relaxed in the theoretical calculations at different pressures. Additionally, the electronic band structures and density of states (DOS) were calculated with the lattice parameters directly taken from the Rietveld refinement.

3. Results and discussion

As shown in Fig. 1, the first pressure-induced structural transition occurred at about 3.3 GPa and completed at 4.1 GPa. Fig. 2a clearly illustrates that a good fitting result was obtained, when the theoretically proposed monoclinic structure (space group $C2/c$) was used to carry out Rietveld refinement of 0.8 GPa [3]. Therefore, the

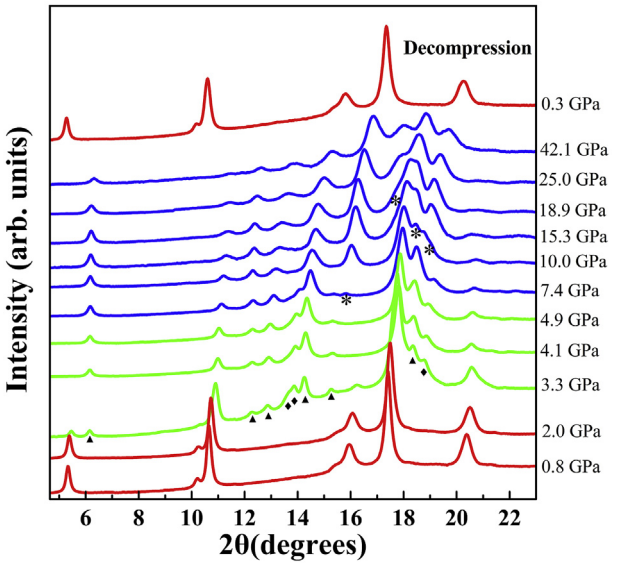

Fig. 1. Angle dispersive X-ray powder diffraction patterns of Cu_2Se under high pressure at room temperature. Diamonds, arrows and asterisks represent new diffraction peaks for phase II, phase III and phase IV, respectively.

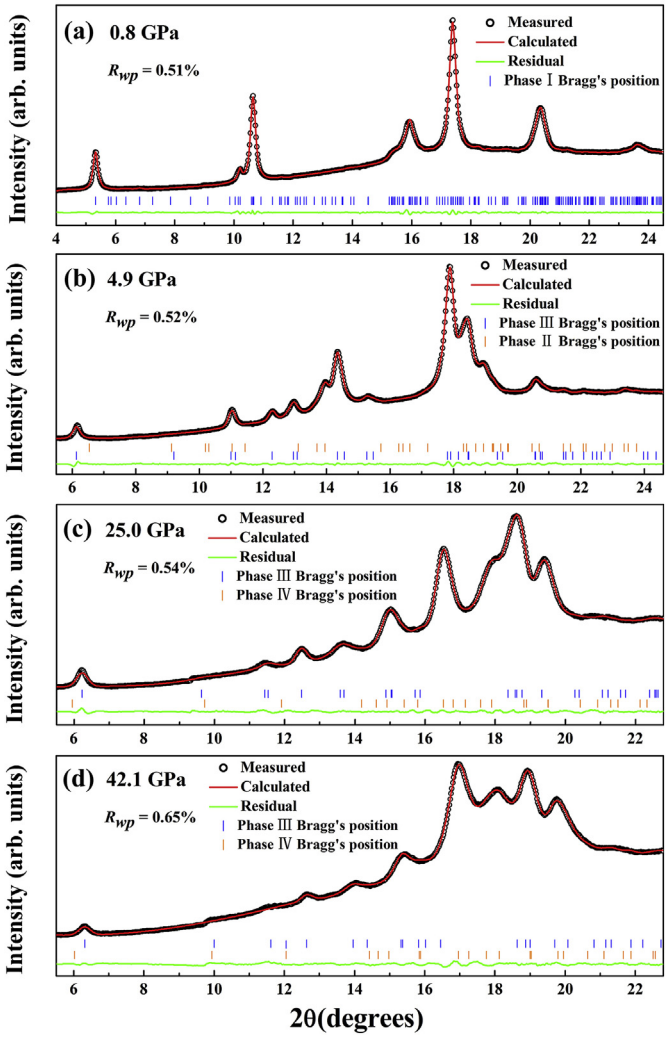

Fig. 2. Rietveld refinement results of (a) 0.8, (b) 4.9, (c) 25.0 and (d) 42.1 GPa, respectively.

initial low-pressure phase of Cu_2Se is assigned to the monoclinic structure reported by Liu et al. [3]. The experimental crystallographic information of Cu_2Se at 0.3, 0.8 and 2.0 GPa, respectively, are shown in the Supplementary Material. To solve the crystal structure of the first high-pressure phase, the structure prediction via CALYPSO methodology was performed at 4.9 GPa [51]. Finally, the best fitting of 4.9 GPa was achieved by the combination of two phases. Here, phase II has a monoclinic structure with space group $C2/m$, which was solved by the previously proposed lowest-energy structure of Cu_2Te at ambient conditions [14]. Phase III is assigned to the most stable structure (space group $C2/m$) proposed by CALYPSO methodology at 4.9 GPa. The related theoretical crystallographic information was collected in the Supplementary material. Fig. 2b shows the Rietveld refinement of 4.9 GPa by the coexistence of phase II and phase III. The relative experimental results of Rietveld refinement were reported in the Supplementary Material. Similarly, the high-pressure study of Ag_2Se by Zhao et al. reports that to fully match the experimental XRD patterns, a metastable $C2/m$ phase needs to be added into the Rietveld refinements, which may be due to the kinetic factors or deviatoric stresses from the quasi-hydrostatic pressure conditions [44]. As observed in Fig. 1, a pressure-induced structural transition started at 7.4 GPa, where new peaks appeared. Moreover, the analysis of ADXRD patterns

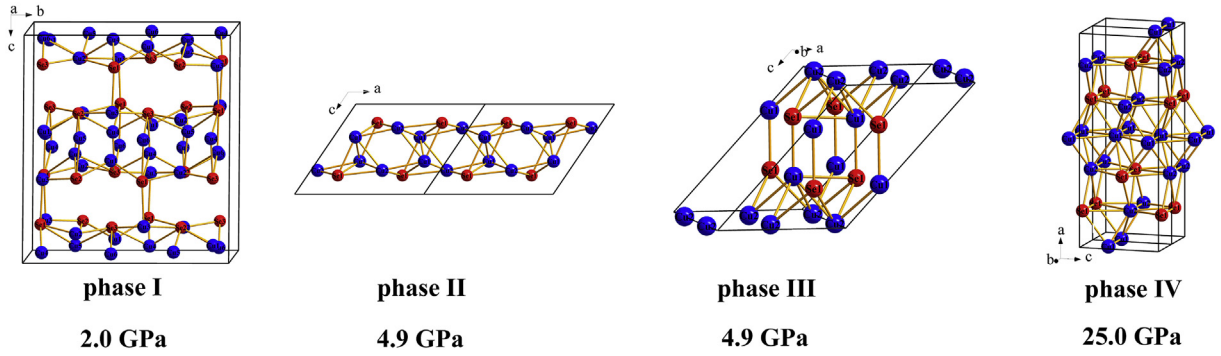

Fig. 3. Structural models of Cu_2Se for all phases.

revealed that phase II disappeared at 10.0 GPa; phase III and phase IV were coexisted up to 42.1 GPa, the highest pressure in this study, which may be due to the non-hydrostatic pressure conditions above 20–25 GPa. Besides, the decompression experiments show that the structural phase transitions are reversible. Phase IV is solved to be an orthorhombic structure with space group $Pca2_1$, through the CALYPSO methodology performed at 42.1 GPa. The related theoretical crystallographic information was located in the Supplementary material. The Rietveld refinement profile of 25.0 and 42.1 GPa was shown in Fig. 2c and d, respectively. The relative experimental results of Rietveld refinement were collected in the Supplementary material.

As observed in Fig. S1, the previous study proposed that the initial phase of Cu_2Se is constructed from stacking layers structure under ambient conditions [3]. Up to 2.0 GPa, the layers were all connected by the formation of Cu3–Se1 ionic-covalent bonds. As shown in Fig. 3, phase II is built up of unique tunnel structures along *b* direction at 4.9 GPa. These tunnels may provide channels for the transfer of the photogenerated electrons and holes, preventing their excessive recombination and enabling more free carries to participate in the photodecomposition process [56]. At 4.9 GPa, phase III contains one-dimensional chains along *b*

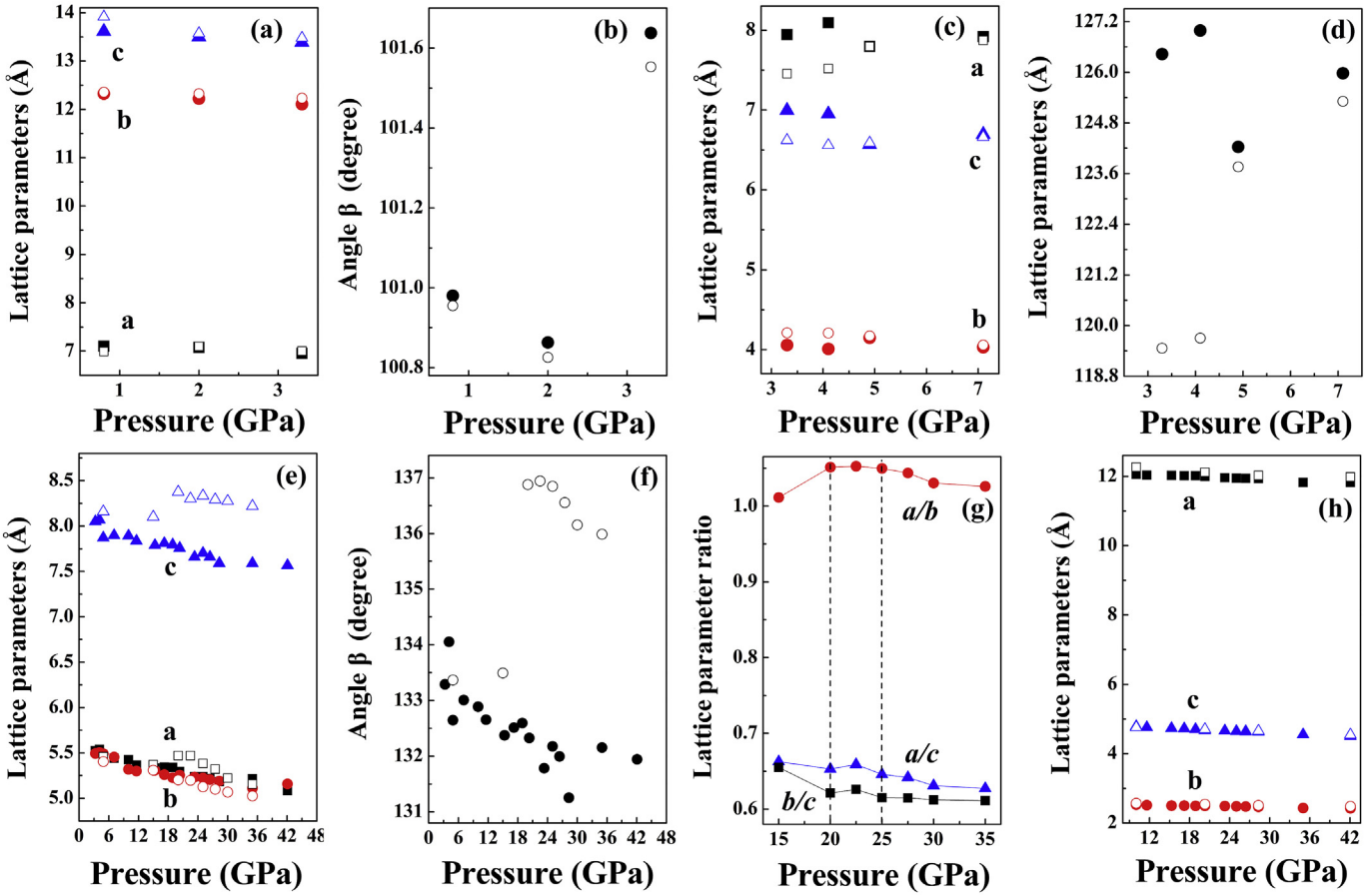

Fig. 4. Lattice parameters of (a) initial phase, (c) phase II, (e) phase III, and (h) phase IV, respectively. Angle β of (b) initial phase, (d) phase II, and (f) phase III, respectively. Errors given by the GSAS EXPGUI package are smaller than the marker sizes. Empty symbols represent the theoretical values. (g) Calculated lattice parameter ratio of phase III (from 15.0 to 35.0 GPa). The solid lines are guide for the eyes.

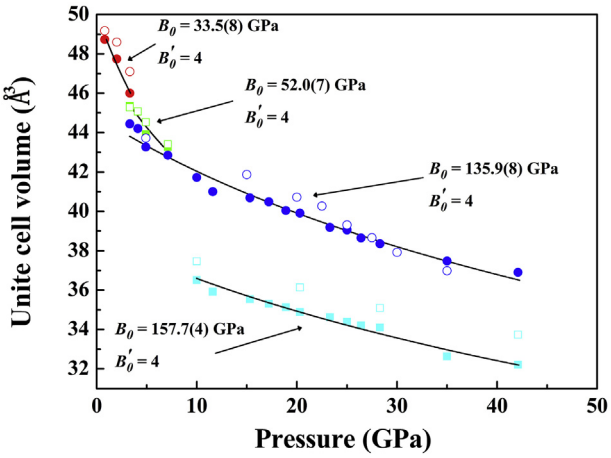

Fig. 5. Pressure dependence of per formula unit volume for all phases of Cu_2Se. Errors given by the GSAS EXPGUI package are smaller than the marker sizes. Empty symbols represent the theoretical values.

direction that are linked together along the *c* direction via Se atoms (see Fig. 3 and Fig. S2). The chain features rhombus (Cu2–Cu1–Cu2–Cu1) clusters which are connected together with Se atoms. For phase III, up to 25.0 GPa, Cu2–Cu2 and Cu1–Se1 bonds also formed within the chains, see Fig. 3 and Fig. S2. As shown in Fig. 3, there is a sheet of Cu1 atoms network in the center of the cell for phase IV.

As shown in Fig. 4a, *b* and *c* directions are more compressible than *a* direction in the initial phase, due to the weak Cu–Se bonds along *b* and *c* directions. As observed in Fig. 4e, *c* direction in phase III is more compressible, due to the weak Cu1–Se1 interactions between the chains (see Fig. 3 and Fig. S2). Kinetic factors or deviatoric stresses may be responsible for the deviation between our theoretical angles and experimental ones for phase III (as shown in Fig. 4f). Besides, we find that the compressibility of calculated lattice parameter ratio of phase III undergoes intense fluctuation at about 20.0–25.0 GPa (see Fig. 4g), which may be attributed to a pressure-induced ETT. As shown in Fig. 4h, *b* and *c* directions in phase IV is more compressible, associated with the weak Cu1–Cu1 interactions in *bc* plane.

Fig. 5 shows the volume per formula unit as a function of pressure for all phases. These *P-V* data are fitted to the usual Birch-Murnaghan (BM) equation of state (EOS) [57]. Here, first-pressure derivative B_0' were fixed at 4 for all the phases. We obtained B_0 = 33.5(8) GPa and V_0 = 50.07(5) Å^3 for the initial low-pressure phase. The lower B_0 is likely related to the high compressibility of *b* and *c* directions. The compression behavior of phase II is determined by the following characteristic parameters: B_0 = 52.0(7) GPa, V_0 = 48.02(6) Å^3. As shown in Fig. 5, the compressibility behaviors is described by B_0 = 135.9(8) GPa (V_0 = 44.84(2) Å^3) for phase III, and B_0 = 157.7(4) GPa (V_0 = 38.72(2) Å^3) for phase IV. There is an obvious volume collapse between phase III and phase IV, which suggests a possible pressure-induced first-order phase transition. Besides, our theoretical calculations of unit cell volume compare not well with experimental ones in phase IV, which may be due to the non-hydrostatic pressure conditions.

In order to determine the electronic band structures for all phases and a possible pressure-induced ETT at about 20.0–25.0 GPa, we carried out first-principles calculations. The previous study has reported that Cu_2Se is an indirect band-gap semiconductor (Eg~1.25–1.5 eV) at ambient pressure [5]. As shown in Fig. 6a, indeed, the initial low-pressure phase is an indirect band-gap semiconductor (Eg = 0.05 eV) at 0.3 GPa, with conduction-band minimum (CBM) at Γ point and valence-band maximum (VBM) located between Γ and *Z* point. Given the underestimated theoretical band-gap, the calculated result was acceptable. As observed in Fig. 6b, the initial low-pressure phase is an indirect band-gap semiconductor (Eg = 0.06 eV) at 2.0 GPa, but the VBM located at *V* point. The significant electron band dispersion

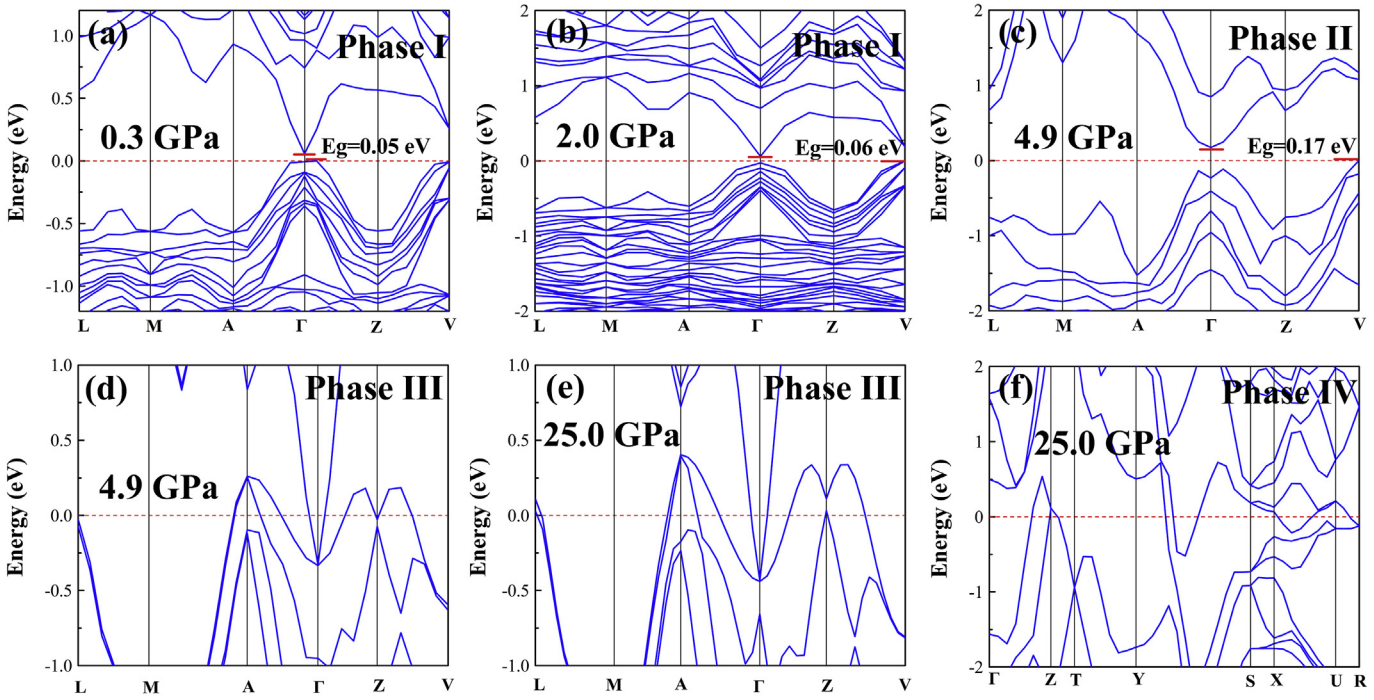

Fig. 6. Calculated band structures of Cu_2Se for (a) initial phase at 0.3 GPa, (b) initial phase at 2.0 GPa, (c) phase II at 4.9 GPa, (d) phase III at 4.9 GPa, (e) phase III at 25.0 GPa, and (f) phase IV at 25.0 GPa, respectively.

is observed along the *Z*-Γ-*A* symmetry line (see Fig. 6a and b). Because mixed carrier transport (electrons and holes) suppresses the Seebeck coefficient, it is necessary to select one type of carrier transport (electron or hole) [58]. Thus, the significant electron band dispersion in the initial phase may lead to a dramatic Seebeck coefficient by the contribution of single carrier (electrons) transport [59]. As shown in Fig. S3, the partial electron density of state (PDOS) and sum DOS results of 2.0 GPa indicate that VBM is mostly dominated by the contributions of Cu-3*d* and Se-4*p* states. As observed in Fig. 6c, phase II is an indirect band-gap semiconductor (Eg = 0.17 eV) at 4.9 GPa, with CBM at Γ point and VBM at *V* point. Fig. S4 shows that the VBM of phase II is mostly composed by Cu1-3*d*, Cu2-3*d* and Se1-4*p* electrons. At 4.9 GPa, phase III shows a semimetallic band structure with four hole bands through the Fermi level at *A* point, Γ-*Z* and *Z*-*V* directions, respectively, see Fig. 6d. The ETT is a consequence of a topological change in the Fermi surface related to the passage of an extremum of the electron energy band (equivalent to the van Hove peak in the density of states) through the Fermi level [60]. As observed in Fig. 6e, the electronic structure of phase III at 25.0 GPa is similar to that of 4.9 GPa, but there are six hole bands through the Fermi level, located at *L* point, *A* point, *Z* point and Γ-*Z*-*V* direction, respectively. Given this evolution in the number of hole bands crossing over the Fermi level, the above mentioned pressure-induced ETT in phase III appears reasonable. Apart from the direct observation of the changes at the Fermi surface by means of angle-resolved photoelectron spectroscopy, transport measurements have also been used as one of the most convincing ways to detect ETTs [15–23,60]. As shown in Fig. 6f, there is a large band overlap in the band structure of phase IV, which indicates a bulk metal state.

4. Conclusions

In summary, we studied the high-pressure behaviors of Cu_2Se up to 42.1 GPa at room temperature through ADXRD measurements and first-principles calculations. The pressure-induced structural transition sequence is identified. The initial low-pressure phase (space group $C2/c$) transformed to phase II (space group $C2/m$) and semimetallic phase III (space group $C2/m$) at 3.3 GPa; and then reconstructed to bulk metallic phase IV (space group $Pca2_1$) at 7.4 GPa. The compressional behaviors of all phases were determined.

Acknowledgments

This work was financially supported by the National Natural Science Foundation of China (Grant Nos. 41572357 and 11704142); and Jilin Province Science and Technology Development Program, China (20170520119JH).

Appendix A. Supplementary data

Supplementary data related to this article can be found at https://doi.org/10.1016/j.jallcom.2017.10.201.

References

[1] H.L. Liu, X. Shi, F.F. Xu, L.L. Zhang, W.Q. Zhang, L.D. Chen, Q. Li, C. Uher, T. Day, G.J. Snyder, Nat. Mater. 11 (2012) 422.
[2] B. Yu, W. Liu, S. Chen, H. Wang, H. Wang, G. Chen, Z. Ren, Nano Energy 1 (2012) 472.
[3] H. Liu, X. Yuan, P. Lu, X. Shi, F. Xu, Y. He, Y. Tang, S. Bai, W. Zhang, L. Chen, Y. Lin, L. Shi, H. Lin, X. Gao, X. Zhang, H. Chi, C. Uher, Adv. Mater. 25 (2013) 6607.
[4] H. Chi, H. Kim, J.C. Thomas, G. Shi, K. Sun, M. Abeykoon, E.S. Bozin, X. Shi, Q. Li, X. Shi, E. Kioupakis, A. Van der Ven, M. Kaviany, C. Uher, Phys. Rev. B 89 (2014) 195209.
[5] A. B. M. O. Islam Al-Mamun, A.H. Bhuiyan, J. Mater. Sci. Mater. Electron. 16 (2005) 263.
[6] K. Yamamoto, S. Kashida, J. Solid State Chem. 93 (1991) 202.
[7] A. Tonejc, A.M. Tonejc, J. Solid State Chem. 39 (1981) 259.
[8] S.A. Danilkin, A. Skomorokhov, A. Hoser, H. Fuess, V. Rajevac, N.N. Bickulova, J. Alloys Compd. 361 (2003) 57.
[9] S.A. Danilkin, Solid State Ionics 180 (2009) 483.
[10] S.A. Danilkina, M. Avdeeva, T. Sakumab, R. Macquartc, C.D. Ling, J. Alloys Compd. 509 (2011) 5460.
[11] S.A. Danilkin, J. Alloys Compd. 467 (2009) 509.
[12] T. Sakuma, K. Shibata, J. Phys. Soc. Japan 58 (1989) 3061.
[13] A.N. Skomorokhov, D.M. Trots, M. Knapp, N.N. Bickulova, H. Fuess, J. Alloys Compd. 421 (2006) 64.
[14] M.C. Nguyen, J.H. Choi, X. Zhao, C.Z. Wang, Z. Zhang, K.M. Ho, Phys. Rev. Lett. 111 (2013) 165502.
[15] Y.H. Zhang, Y. Li, Y.M. Ma, Y.W. Li, G.H. Li, X.C. Shao, H. Wang, T. Cui, X. Wang, P.W. Zhu, Sci. Rep. 5 (2015) 14681.
[16] M. Jacobsen, S. Sinogeikin, R. Kumar, A. Cornelius, J. Phys. Chem. Solids 73 (2012) 1154.
[17] Y.H. Zhang, Y.M. Ma, A.H. Geng, C.Y. Zhu, G.T. Liu, Q. Tao, F. Li, Q.L. Wang, Y. Li, X. Wang, P.W. Zhu, J. Alloys Compd. 685 (2016) 551.
[18] S.V. Ovsyannikov, V.V. Shchennikov, Chem. Mater. 22 (2010) 635.
[19] F.J. Manjón, R. Vilaplana, O. Gomis, E. Pérez-González, D. Santamaría-Pérez, V. Marín-Borrás, A. Segura, J. González, P. Rodríguez-Hernández, A. Muñoz, C. Drasar, V. Kucek, V. Muñoz-Sanjosé, Phys. Status Solidi B 250 (2013) 669.
[20] E. Itskevich, L. Kashirskaya, V. Kraidenov, Semiconductors 31 (1997) 276.
[21] C.N. Shekar, D. Polvani, J. Meng, J. Badding, Phys. B 358 (2005) 14.
[22] N. Sakai, H. Fritzsche, Phys. Rev. B 15 (1977) 973.
[23] T.J. Scheidemantel, J.F. Meng, J.V. Badding, J. Phys. Chem. Solids 66 (2005) 1744.
[24] Y.H. Zhang, L.Y. Song, X.C. Shao, Y. Li, P.W. Zhu, H.L. Xu, J.Y. Yang, J. Alloys Compd. 715 (2017) 237.
[25] X.J. Chen, V.V. Struzhkin, Y. Yu, A.F. Goncharov, C.T. Lin, H.K. Mao, R.J. Hemley, Nature 466 (2010) 950.
[26] S. Sadewasser, J.S. Schilling, A.P. Paulikas, B.W. Veal, Phys. Rev. B 61 (2000) 741.
[27] X.J. Chen, V.V. Struzhkin, R.J. Hemley, H.K. Mao, C. Kendziora, Phys. Rev. B 70 (2004) 214502.
[28] R. Kubiak, K. Westerholt, H. Bach, Phys. C 166 (1990) 523.
[29] L. Gao, Y.Y. Xue, F. Chen, Q. Xiong, R.L. Meng, D. Ramirez, C.W. Chu, J.H. Eggert, H.K. Mao, Phys. Rev. B 50 (1994) 4260.
[30] A. Sacchetti, E. Arcangeletti, A. Perucchi, L. Baldassarre, P. Postorino, S. Lupi, N. Ru, I.R. Fisher, L. Degiorgi, Phys. Rev. Lett. 98 (2007) 026401.
[31] M. Houcker, M. v. Zimmermann, M. Debessai, J.S. Schilling, J.M. Tranquada, G.D. Gu, Phys. Rev. Lett. 104 (2010) 057004.
[32] M. Abdel-Hafiez, X.-M. Zhao, A.A. Kordyuk, Y.-W. Fang, B. Pan, Z. He, C.-G. Duan, J. Zhao, X.-J. Chen, Sci. Rep. 6 (2016) 31824.
[33] H. Suderow, V.G. Tissen, J.P. Brison, J.L. Martínez, S. Vieira, Phys. Rev. Lett. 95 (2005) 117006.
[34] D.C. Freitas, P. Rodière, M.R. Osorio, E. Navarro-Moratalla, N.M. Nemes, V.G. Tissen, L. Cario, E. Coronado, M. García-Hernández, S. Vieira, M. Núñez-Regueiro, H. Suderow, Phys. Rev. B 93 (2016) 184512.
[35] C. Berthier, P. Molinié, D. Jérome, Solid State Commun. 18 (1976) 1393.
[36] Y.I. Joe, X.M. Chen, P. Ghaemi, K.D. Finkelstein, G.A. de la Pea, Y. Gan, J.C.T. Lee, S. Yuan, J. Geck, G.J. MacDougall, T.C. Chiang, S.L. Cooper, E. Fradkin, P. Abbamonte, Nat. Phys. 10 (2014) 421.
[37] Y. Chen, J. Analytis, J.H. Chu, Z. Liu, S.K. Mo, X.L. Qi, H. Zhang, D. Lu, X. Dai, Z. Fang, Science 325 (2009) 178.
[38] H. Zhang, C.X. Liu, X.L. Qi, X. Dai, Z. Fang, S.C. Zhang, Nat. Phys. 5 (2009) 438.
[39] X.L. Qi, S.C. Zhang, Rev. Mod. Phys. 83 (2011) 1057.
[40] B. Yan, S.C. Zhang, Rep. Prog. Phys. 75 (2012) 96501.
[41] W. Zhang, R. Yu, W. Feng, Y. Yao, H. Weng, X. Dai, Z. Fang, Phys. Rev. Lett. 106 (2011) 156808.
[42] A. Sulaev, P. Ren, B. Xia, Q.H. Lin, T. Yu, C. Qiu, S.Y. Zhang, M.Y. Han, Z.P. Li, W.G. Zhu, Q. Wu, Y.P. Feng, L. Shen, S.Q. Shen, L. Wang, AIP Adv. 3 (2013) 032123.
[43] Z. Zhao, S. Wang, H. Zhang, W.L. Mao, Phys. Rev. B 88 (2013) 024120.
[44] Z. Zhao, S. Wang, A.R. Oganov, P.C. Chen, Z.X. Liu, W.L. Mao, Phys. Rev. B 89 (2014) 180102.
[45] P. Naumov, O. Barkalov, H. Mirhosseini, C. Felser, S.A. Medvedev, J. Phys. Condens. Matter 28 (2016) 385801.
[46] R. Murray, R. Heyding, Can. J. Chem. 53 (1975) 878.
[47] J. Zhu, Q. Li, L. Bai, Y. Sun, M. Zhou, Y. Xie, Chem. Eur J. 18 (2012) 13213.
[48] A.P. Hammersley, S.O. Svensson, M. Hanfl, A.N. Fitch, D. Hausermann, High. Press. Res. 14 (1996) 235.
[49] A.C. Larson, R.B. Von Dreele, General Structure Analysis System, LANSCE, MS-H805, Los Alamos, New Mexico, 1994.
[50] B.H. Toby, J. Appl. Crystallogr. 34 (2001) 210.
[51] Y. Wang, J. Lv, L. Zhu, Y. Ma, Phys. Rev. B 82 (2010) 094116.
[52] G. Kresse, J. Furthmüller, Phys. Rev. B 54 (1996) 11169.
[53] J.P. Perdew, K. Burke, M. Ernzerhof, Phys. Rev. Lett. 77 (1996) 3865.
[54] G. Kresse, D. Joubert, Phys. Rev. B 59 (1999) 1758.
[55] P.E. Blöchl, Phys. Rev. B 50 (1994) 17953.
[56] A.L.J. Pereira, J.A. Sans, R. Vilaplana, O. Gomis, F.J. Manjón, P. Rodríguez-Hernández, A. Muñoz, C. Popescu, A. Beltrán, J. Phys. Chem. C 118 (2014)

23189.
[57] F. Birch, J. Appl. Phys. 9 (1938) 279.
[58] J.-S. Rhyee, K.H. Lee, S.M. Lee, E. Cho, S.I. Kim, E. Lee, Y.S. Kwon, J.H. Shim, G. Kotliar, Nature 459 (2009) 965.
[59] J. Rhyee, E. Cho, K.H. Lee, S.M. Lee, S.I. Kim, H. Kim, Y.S. Kwon, S.J. Kim, Appl. Phys. Lett. 95 (2009) 212106.
[60] R. Vilaplana, J.A. Sans, F.J. Manjon, A. Andrada-Chacon, J. Sanchez-Benítez, O. Gomis, A.L.J. Pereira, B. García-Domene, P. Rodríguez-Hernandez, A. Munoz, D. Daisenberger, O. Oeckler, J. Alloys Compd. 685 (2016) 962.